HSM2025-44924

EXPERIMENTAL BURR ANALYSIS FOR TI-6AL-4V DRILLING APPLICATION

B. DEBARD[1], M. CHERIF*[1], P. A. REY[1]

[1]Univ. Bordeaux, CNRS, Bordeaux INP, I2M, UMR 5295, F-33400, Talence, France

Arts et Metiers Institute of Technology, CNRS, Bordeaux INP, I2M, UMR 5295, F-33400 Talence

*Corresponding author; e-mail: mehdi.cherif@ensam.eu

Abstract

To improve aerostructures assembly processes, aircraft manufacturers want to implement a One-Way Assembly strategy that eliminates the disassembly, cleaning and deburring phases currently required. Implementing this innovative strategy represents major technical challenges, including the management of burr formation at stack interfaces, as they have a negative impact on the assemblies' fatigue strength. Despite extensive research, the burr formation phenomenon remains poorly understood. This paper presents an interrupted experimental design to investigate the burr formation during the drilling process of Ti-6Al-4V alloy. Analysis of burr geometry and microstructures is complemented by cutting force results for three different drilling tool geometries.

Keywords:
Drilling process, Burr formation, Ti-6Al-4V, Cutting force, Tool geometry, EBSD

1 INTRODUCTION

Hybrid structures with low density/stiffness ratios are often used to improve aircraft performance. These structures are generally made of low-density materials such as titanium, aluminium and Carbon Fiber-Reinforced Polymer (CFRP). The mechanical assembly of aerospace structures uses rivets and bolts that require numerous holes to be drilled in the materials making up the stack. The drilling of metallic parts, especially the Ti-6Al-4V alloy, can generates burrs at the stack interfaces, which can affect the fatigue performance of aeronautical structures [Abdelhafeez et al. 2018]. In fact, the material constituting the burr is severely damaged and contains numerous microcracks that lead to significant geometric variations [Régnier et al. 2018]. Consequently, the aerospace industry needs to implement effective burr monitoring strategies to ensure the mechanical performance of hybrid structures, such as defining acceptance limit criteria for the burr size. Burr removal is a costly operation with no added value. Indeed, several operations are required, such as disassembly of structures, cleaning, deburring and reassembly. An alternative strategy, called One-Way Assembly (OWA), is to install the final fastener immediately after the drilling operation, without deburring. This strategy represents an industrial challenge to keep the burr height within a specified criterion. This problematic is particularly relevant for the Ti-6Al-4V alloy.

The phenomenon of burr formation in drilling has been the subject of many studies since the 1970s. [Gillespie 1973] defines four basic burr types representing the mechanisms that can occur during the burr formation: the Cut-Off burr (Fig. 1a), the Poisson burr (Fig. 1b), the Roll-Over burr (Fig. 1c) and the Tear burr (Fig. 1d). [Gillespie 1976a] describes the exit burr formation of a hole as the elongation of the material until failure (Tear burr). The failure point can be reached in front of the tool tip or at the corners of the tool (Fig. 2). When drilling Ti-6Al-4V alloy, material failure predominantly occurs at the corners of the tool [Dornfeld et al. 1999], as shown in Fig. 2. The burr morphology depends on the mechanism involved and the drilling conditions [Eynian et al. 2017].

In the literature, the investigation of the exit burr formation phenomenon generally results in a qualitative analysis using high-speed camera [Bahçe 2019].

In general, studies on metallic burrs have focused on investigating the effect of numerous variables on the burr geometry (height and width), including material properties, workpiece geometry, tool geometry, cutting parameters and lubrication [Frutos Taravillo et al. 2025]. They identified the existence of different burr geometries that are highly dependent on the material ductility [Gillespie 1976a], the feed rate [Bahçe 2019] and the lubrication type [Rodriguez 2024]. Studies investigating the influence of the tool geometry mainly focus on the main characteristics of a drill bit (e.g. diameter, point angle, helix angle, etc…) [Dornfeld et al. 1999]. Only few of them are interested in significant modifications of the tool macro-geometry, such as the addition of chamfers on the tool corners [Franczyk et al. 2020].

Most of the time, studies examine the metallic exit burrs produced during the drilling process at the macroscopic scale, focusing only on the burr geometry. The material

deformation at the microscopic scale is rarely analysed. [Gillespie 1976b] presents a qualitative analysis of an exit burr and a burr cap cross-sections. [Cantero et al. 2005] highlight severe deformation of the material in the vicinity of the burr with a large thermally affected area in Ti-6Al-4V dry drilling. [Eynian et al. 2017] investigate the influence of artificial tool wear on the morphology of a Ti-6Al-4V burr. [Debard et al. 2025] show an increase in deformed material with tool wear in Ti-6Al-4V alloy drilling using exit surface scanning and cross-sectional measurements. However, the above studies don't compare different tool geometries with respect to burr formation mechanisms at the microscopic scale.

This paper presents a multi-scale analysis of the burr formation mechanisms and burr morphology of three different cutting tools. Interrupted tests with cutting force measurements and micrographic analysis of the hole cross-sections were performed, allowing an in-depth comparison of the burr formation phenomenon. Finally, EBSD analyses were carried out to estimate the mechanically affected zone.
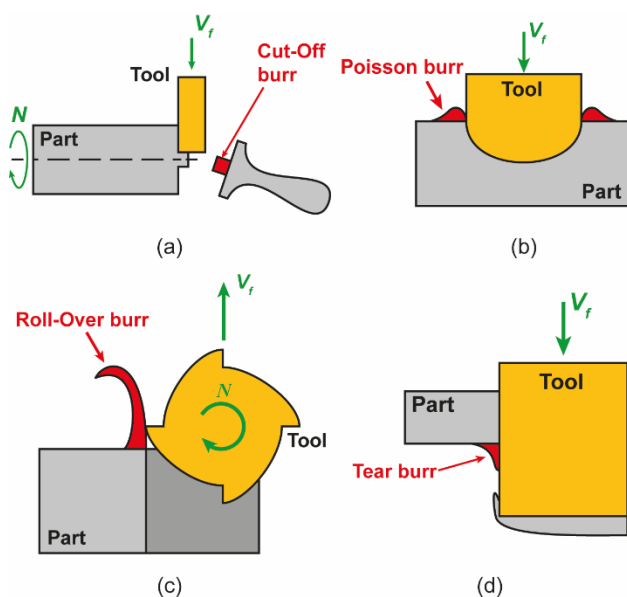

Fig. 1: Formation of a Cut-Off burr (a), Poisson burr (b), Roll-Over burr (c) and Tear burr (d) [Debard et al. 2025]
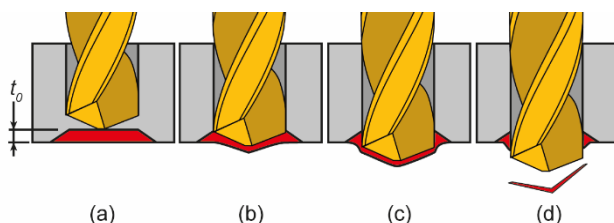

Fig. 2: Exit burr formation in drilling [Debard et al. 2024]

2 MATERIALS AND METHODS

2.1 Materials

All drilling experiments were carried out on a CNC machine equipped with a rotational force sensor (Kistler 9171A). The sample was a 6.1 mm thick Ti-6Al-4V alloy plate. All the tools used are described in Fig .3 The tool 1, that is used in [Debard et al. 2025], has a basic geometry. The tool 2 has specific large chamfers at corners (more than 1 mm height) with a low angle (less than 10°). The tool 3 has a 180° point angle and chamfers at tool corners (angle 30°, height 0.3 mm).

Several post-mortem measurements were performed to investigate the burr formation. The exit surface was scanned using a confocal microscope (Brüker Alicona Infinite Focus G5plus) at each step (cf. protocol section). The average burr height and width were calculated from six measurements on the final hole of each tool. Cross-sections of burrs and during burr formation were obtained by wire EDM (electrical discharge machining). The microstructure was revealed by a chemical preparation (Kroll) and analysed with an optical microscope (Keyence VHX-7000). EBSD measurements (Oxford Instrument) were carried out on these cross-sections.
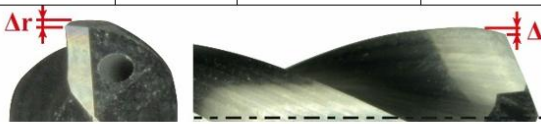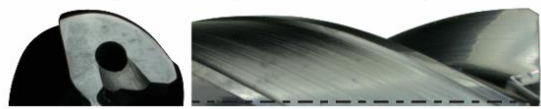

Tool 1 [Debard et al. 2025]			
Ø [mm]	Coating	Point angle [°]	Chamfer [°]
6.35	TiAlN	140	-

Tool 2			
Ø [mm]	Coating	Point angle [°]	Chamfer [°]
6.35	-	135	< 10

Tool 3			
Ø [mm]	Coating	Point angle [°]	Chamfer [°]
6.3	TiAlN	180	30

Fig. 3: *Description of tools used during experiments*

2.2 Protocol

To observe the formation of the burr, interrupted drilling tests were carried out for each tool. These tests consist in stopping the process at different depths (Fig. 4). This allows the deformation induced by the tool to be observed. The list of depths is given in Tab. 1. The tool 3 has different steps due to its 180° point angle.

Tests were carried out with a cutting speed set to 25 m/min, a feed rate to 0.06 mm/rev and MQL (Minimum Quantity Lubricant).

Tab. 1: Depth steps during interrupted tests

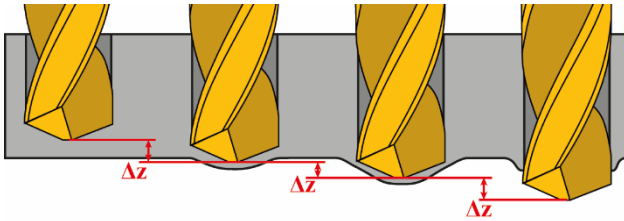| Step	1	2	3	4	5	6	7	8	9	10	11	12	13	14	15	16
Depth for tool 1 and 2 [mm]	5.8	6	6.15	6.3	6.45	6.6	6.75	6.9	7.05	7.2	7.35	7.5	7.65	7.8	8	9
Depth for tool 3 [mm]	5.7	5.8	5.9	6	6.15	6.3	6.45	6.6	-	-	-	-	-	-	-	-

*Fig. 4: Interrupted tests [Debard et al. 2025]*

3 RESULTS AND DISCUSSION

### 3.1 Cutting forces comparison

The cutting forces of each tool are shown in Fig. 5. On these graphs, the X axis is the depth of the tool tip in the material. Thus, 0 mm is when the tip touches the entry surface, and 6.1 mm is when it reaches the exit surface.

As expected, the tool 3 generates the highest axial force F_z (Fig. 5a), which is more than twice the axial force generated by the tool 2. The tool 2 generates the lowest axial force. This is due to its web thinning and its small edge acuity radius (around 10 µm). Moreover, the 180° point angle of the tool 3 induces radial vibrations of the tool as it penetrates the material. These vibrations can be observed on the axial force curve up to a depth of 1.7 mm.

On the other hand, the maximum cutting torque M_z is generated by the tool 2 (Fig. 5b). This is due to the tool chamfers, that contribute to more than 50 % of the total torque (from 1.15 mm to 3.4 mm). These chamfers also induce a residual torque after 7 mm. This is explained in more detail in the burr formation analysis section. Thus, the tool 1 generates the lowest cutting torque.
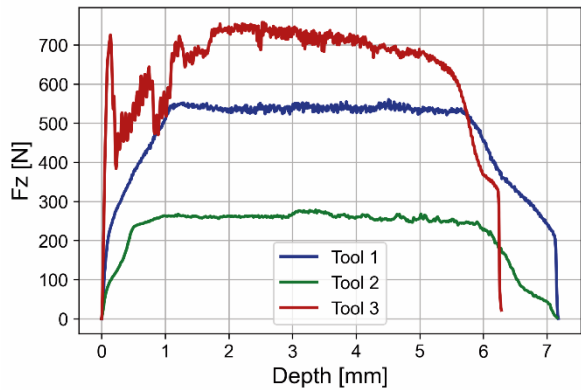
(a)
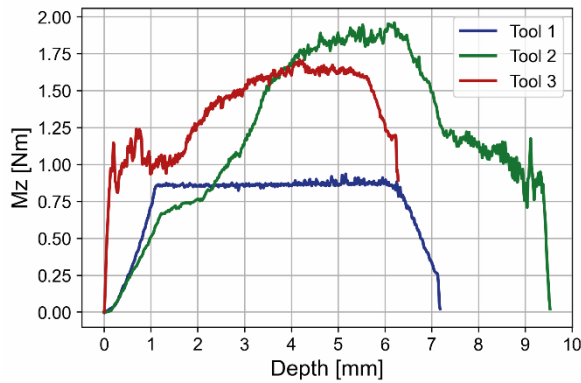
(b)

Fig. 5: Axial cutting force F_z (a) and cutting torque M_z (b) for all tools

3.2 Burr formation analysis

Burr formation steps

The Fig. 6 shows the burr formation on the exit surface induced by each tool. As expected, each burr formation starts with the formation of a burr cap in front of the tool. The onset of the burr formation is characterised by a decrease in the axial cutting force F_z. As shown in Fig. 5a, all burr formation starts before the 6.1 mm depth, which is the thickness of the specimen. It is important to note that the decrease in cutting torque M_z (Fig. 5b) starts later, as the tool tip generates a high axial cutting force but no torque.

The burr cap can be removed at different depths depending on the tool geometry, as shown in Fig. 6. This depth is characterised by drastic reduction in the axial cutting force F_z. Sometimes the fracture occurs at the same time as the burr is formed, as observed with the tool 1 and the tool 3. In these cases, there is also a significant reduction of the cutting torque M_z.

The failure of the material can also occur before that the burr is formed. Indeed, for the tool 2, the burr cap is removed at a depth of 6.9 mm, but this is not the end of the burr formation. After that depth, there is a phase of fragmentation of the exit surface. This phase lasts until the tool corners reach the exit surface (from 7.05 mm to 7.2 mm). Then, the tool chamfers deform the material until the tool exits the specimen (9 mm depth). These phases are characterised by a residual cutting torque M_z while the axial cutting force F_z is zero. The residual cutting torque M_z (more than 1 Nm) observed in the Fig. 5b for the tool 2 confirms an interaction between the tool and the material after removing the burr cap. There is then a sharp reduction in the cutting torque M_z to zero, which is characteristic of the time sequence when the tool completely exits the material. The burr is generated at this depth (2 mm after removing the burr cap).
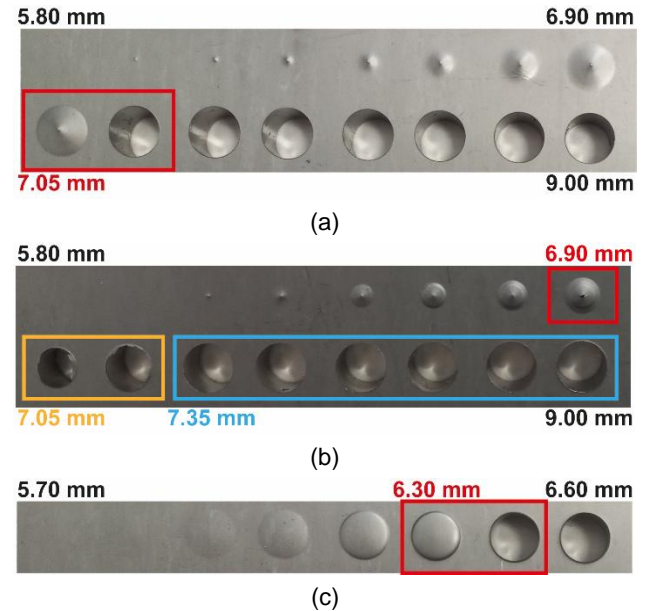

(a)

(b)

(c)

Fig. 6: Exit burr formation induced by the tool 1 (a), 2 (b) and 3 (c)

Burr cap morphology

As mentioned in the introduction, each tool forms a cap during the burr formation. The Fig. 7 shows the cross-sections of the holes just before the burr cap is removed for each tool. The tool 1 (Fig. 7a) produces a cap with a conical shape. The cone angle is the same as the point angle of the

drill bit. The cap is thicker at the tip than at the corners of the tool and has an average thickness of 106 µm. Apart from the tip, the variation in thickness is less than 10 %. The burr cap produced by the tool 2 (Fig. 7b) also has a conical shape. However, its thickness is less than that of the burr cap formed by the tool 1. Its thickness is between 15 µm and 30 µm. Contrary to these tools, the tool 3 generates a flat burr cap (Fig. 7c) with a large variation in thickness. The thickness is equal to 550 µm at the tool tip and then decreases continuously to 70 µm at the corners of the tool. The resulting average thickness is equal to 410 µm.

These results show the influence of the tool macro-geometry on the burr cap and on the volume of deformed material. The shape of the cap depends on the point angle of the drill bit. A 180° point angle results in a high cap thickness at the tool tip and a relatively low thickness at the tool corners, while a lower point angle results in a more uniform thickness along the radius. Changing the cap shape also changes the stress field in front of the tool. Thus, the shape of the cap influences the fracture pattern on the exit surface and therefore the mechanisms that form the burr.

In addition, the average burr cap thickness appears to be related to the axial cutting force F_z, since both increase at the same time. However, the nominal axial cutting force is not sufficient to determine the burr cap thickness. Indeed, when the axial force is multiplied by 2.1 (tool 2 and 1), the average cap thickness is multiplied by 3.8. On the other hand, when comparing the tool 1 and the tool 3, the nominal axial cutting force is multiplied by 1.3 while the average burr cap thickness is multiplied by more than 3.9. This shows that the nominal axial cutting force is not sufficient to determine the burr cap thickness.
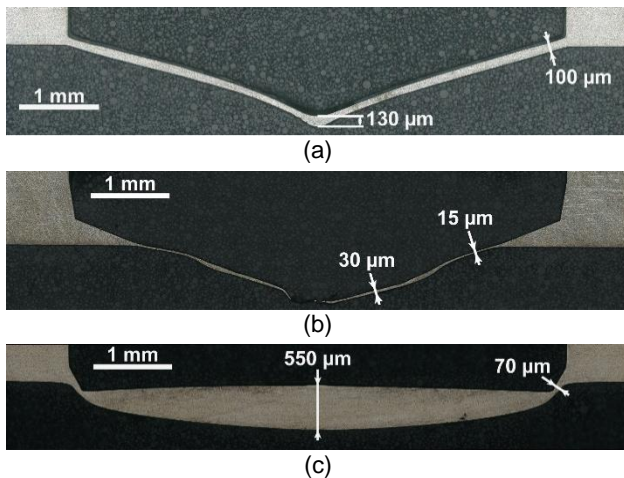

(a)

(b)

(c)

Fig. 7: Cross-sections during the burr formation of the tool 1 at 7.05 mm depth (a), the tool 2 at 6.9 mm depth (b) and the tool 3 at 6.3 mm depth (c)

3.3 Burr analysis

Burr morphology

The Fig. 8 shows the morphologies of the burrs generated by each tool. The microstructure of the material can also be observed in this figure. These cross-sections show three different burr morphologies depending on the tool used. This highlights the differences in the burr formation mechanisms.

The burr produced by the tool 1 (Fig. 8a) is small, with a median height of 57 µm and a median width of 66 µm. The microstructure of the burr shows severe deformations at the drill hole. It is oriented in the same direction as the feed (vertical), whereas it should be oriented in the rolling

direction (horizontal). It shows that there is no more cutting at the end of the burr formation. The burr appears to be produced by stretching the material to failure, as illustrated in the Fig. 2.
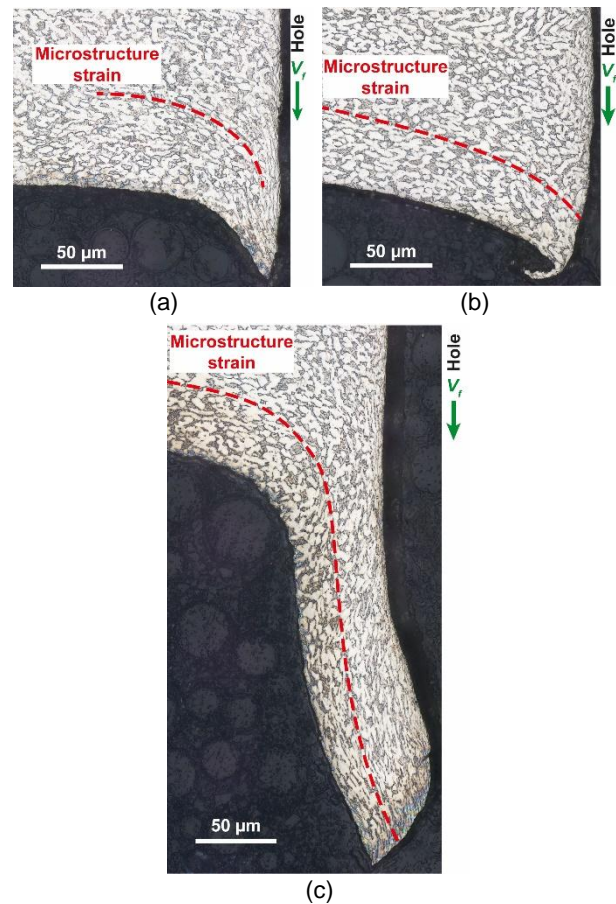

(a)

(b)

(c)

Fig. 8: Burr morphology produced by the tool 1 (a), 2 (b) and 3 (c)

The tool 2 generates a burr (Fig. 8b) that is completely different from the previous one. This burr is small (75 µm median height) but large (260 µm median width) and looks like a Roll-Over burr (Fig. 1c). Unlike the burr produced by the tool 1, there is no severe deformation of the microstructure. It is deformed but stops right at the hole surface. It therefore appears that the cutting never stops during the burr formation, and so that the burr is induced by the cutting of the material by the tool chamfers and not by its elongation.

The burr produced by the tool 3 is shown in Fig. 8c. This burr is tall (253 µm median height) and large (320 µm median width). The morphology of the burr highlights a particular burr formation. The burr formation steps are detailed in the Fig. 9. The failure of the burr cap occurs after the elongation of the material along the chamfer at the tool corners (Fig. 9a). The burr is then straightened as the tool keeps moving forward (Fig. 9b). When the tool is pulled out, the burr curves towards the inside of the hole (Fig. 9c). This results in a tall and thin curved burr.

These results demonstrate the significant influence of the tool macro-geometry on the burr formation mechanisms and on the burr morphology. However, it is not possible to correlate the cutting forces, the burr cap thickness and the burr size for different tools. Indeed, while the axial cutting force F_z and the average burr cap thickness induced by the tool 2 are lower than those induced by the tool 1, the burrs generated by the tool 2 are bigger than those generated by

the tool 1. The opposite behaviour is observed for the tool 1 and the tool 3. The tool 2 also generates the highest cutting torque M_z, but not the tallest or the largest burr.
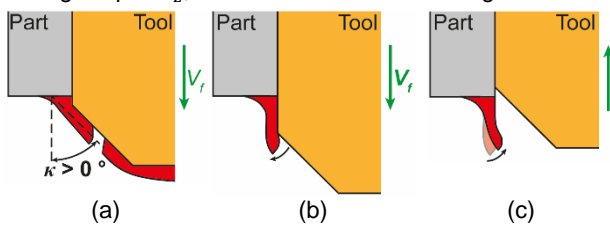

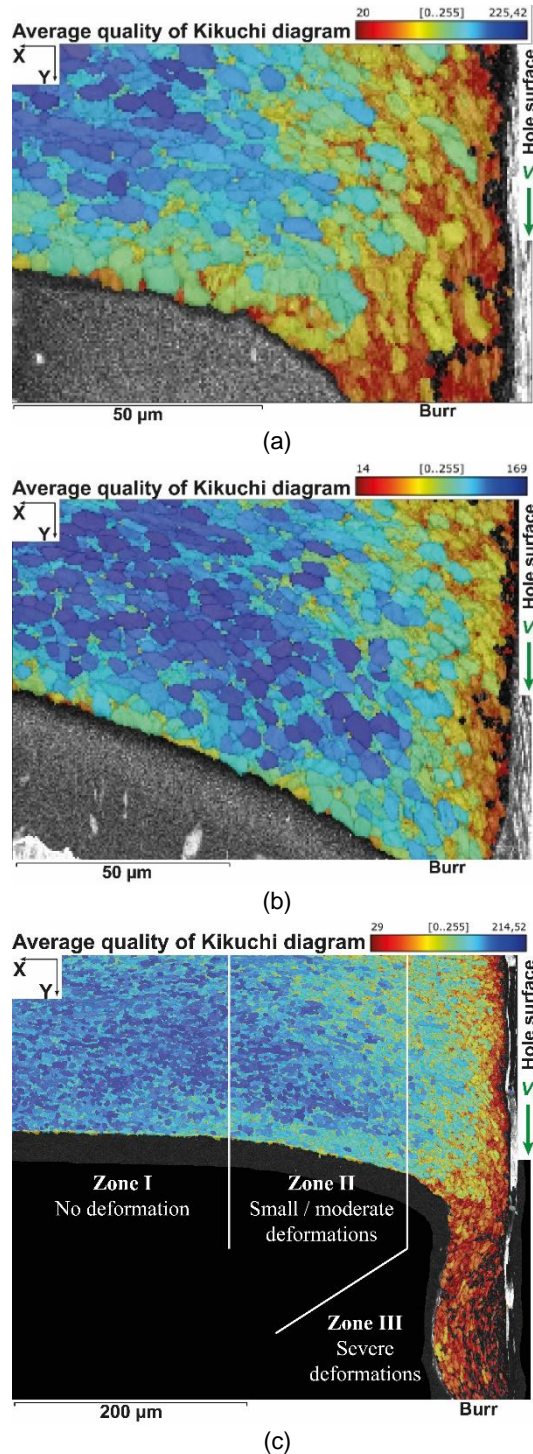Fig. 9: Burr formation steps generated by the tool 3

(a)

(b)

(c)

Fig. 10: Strain levels of the material around the burr generated by the tool 1 (a), 2 (b) and 3 (c)

Affected area close to the burr

To complete the analysis of the burr formation, EBSD measurements were carried out. These measurements provide information on the crystallographic orientation and the strain level of a grain from its Kikuchi diagram. It is possible to relatively compare the strain level of grains on one measurement by comparing the quality of each Kikuchi diagram, as it is influenced by the number of dislocations. So, a lower quality indicates a higher strain level and vice versa.

The Fig. 10 shows the strain level cartographies of the burrs produced by each tool. The Fig. 10a shows the burr formed by the tool 1. It shows the presence of severe deformations inside the burr and near the hole surface, especially where the material has been stretched. On the other hand, the cartography of the burr produced by the tool 2 (Fig. 10b) shows less deformation. They are localised at the hole surface, but not in the burr. The material appears to be less deformed with the tool 2 than with the tool 1. The cartography of the burr produced by the tool 3 (Fig. 10c) is similar to that of the tool 1 (Fig. 10a), with severe deformations observed inside the burr and close to the hole surface.

This last cartography (Fig. 10c) also allows to distinguish three different areas. The boundaries of these areas can be defined radially from the hole surface. The area furthest from the hole surface is the Zone I, that is not affected by the burr formation and is therefore not deformed. Then, there is the Zone II that contains moderate deformations induced by the burr formation. The radial boundary between the Zone I and the Zone II is equal to the width of the burr. The area closest to the hole surface is the Zone III. This area contains the most severe deformations of the material induced by the burr formation. Its boundary is difficult to determine from the burr size, but appears to be close to the burr thickness. In some cases, such as the burr produced by the tool 2, the Zone III is very small or even non-existent.
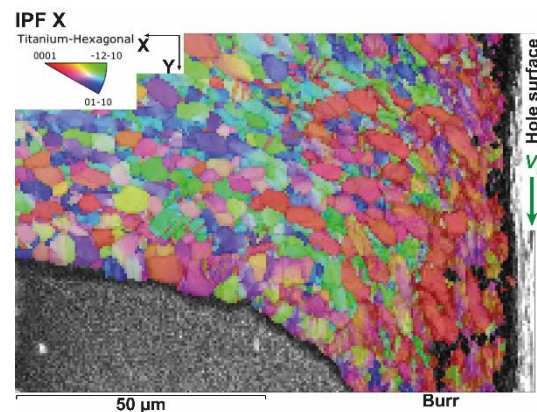

Fig. 11: IPF of the X axis cartography of the burr formed by the tool 1

The Fig. 11 shows the Inverse Pole Figure (IPF) cartography in relation to the X axis of the burr produced by the tool 1. It shows how the X axis of the measurement is oriented in comparison with the α-phase crystal of the titanium (hexagonal pseudo-compact). In the Zone I, a random distribution can be observed, corresponding to the undeformed material. However, close to the hole surface and the burr, the cartography shows a preferred orientation of the crystal structure. This crystallographic texture is induced by the severe deformations that occur during the burr formation in the Zone III.

Among these three areas, the Zone III is probably the one that has the highest influence on the mechanical properties

of the material. In this area, the burr formation induces severe deformations of the material, which is associated with the appearance of a oriented crystallographic texture.

4 CONCLUSION

This paper investigates the influence of the tool macro-geometry on the burr formation when drilling Ti-6Al-4V alloys. Interrupted tests were carried out to study the burr formation steps depending on the tool geometry. The results presented in this paper helped to improve the understanding of the burr formation phenomenon. The main conclusions are as follows:

- The start of the burr formation is characterized by a decrease in the axial cutting force F_z. When it reaches zero, the burr cap is removed. The burr formation ends when the cutting torque M_z is zero.

- The shape of the burr cap depends on the drill bit point angle. The nominal axial cutting force is not sufficient to determine the thickness of the burr cap.

- The macro-geometry of the tool has a strong influence on the mechanisms involved in the burr formation. Thus, the use of different tools can result in different burr morphologies.

- The phenomenon of burr formation induces several levels of deformation in the material. Three areas have been identified. The Zone III contains the most severe deformations in addition to the appearance of a specifically oriented crystallographic texture.

5 ACKNOWLEDGEMENTS

6 REFERENCES

[Abdelhafeez et al. 2018] Abdelhafeez, A.M., Soo, S.L., Aspinwall, D.K., Dowson, A., Arnold, D. The influence of burr formation and feed rate on the fatigue life of drilled titanium and aluminium alloys used in aircraft manufacture. CIRP Annals, January 2018, Vol.67, pp 103–108, ISSN 0007-8506

[Bahçe 2019] Bahçe, E., Özdemir, B. Investigation of the burr formation during the drilling of free-form surfaces in Al 7075 alloy. Journal of Materials Research and Technology, September 2019, Vol.8, pp 4198–4208, ISSN 22387854

[Debard et al. 2024] Debard, B., Rey, P.A., Cherif, M., Chiron, T., Sommier, A., Chavatte, T. Experimental analysis of burr formation during Ti6Al4V drilling. Materials Research Proceedings, April 2024, Vol.41, pp 2065–2074

[Debard et al. 2025] Debard, B., Rey, P.A., Cherif, M. Investigation of burr formation in Ti-6Al-4V drilling. Journal of Manufacturing Processes, 2025, Vol.142, pp 482–493, ISSN 1526-6125

[Dornfeld et al. 1999] Dornfeld, D.A., Kim, J.S., Dechow, H., Hewson, J., Chen, L.J. Drilling Burr Formation in Titanium Alloy, Ti-6Al-4V. CIRP Annals, 1999, Vol.48, pp 73–76, ISSN 00078506

[Eynian et al. 2017] Eynian, M., Das, K., Wretland, A. Effect of tool wear on quality in drilling of titanium alloy Ti6Al4V, Part I: Cutting Forces, Burr Formation, Surface Quality and Defects. High Speed Machining, January 2017, Vol.3, pp 1–10, ISSN 22993975

[Franczyk et al. 2020] Franczyk, E., Ślusarczyk, Ł., Zębala, W. Drilling Burr Minimization by Changing Drill Geometry. Materials, Jully 2020, Vol.13, pp 3207, ISSN 1996-1944

[Frutos Taravillo et al. 2025] Frutos Taravillo, S., Paroissien, E., Landon, Y., Schwartz, S., Fressinet, M., Chirol, C. A Review on Metallic Drilling Burrs: Geometry, Formation, and Effect on the Mechanical Strength of Metallic Assemblies. Journal of Manufacturing Science and Engineering, April 2025, Vol.147, ISSN 1087-1357

[Gillespie 1973] Gillespie, L.K., Blotter, P.T. The Formation and Properties of Machining Burrs. Journal of Engineering for Industry, 1973, Vol.98, pp 66–74, ISSN 0022-0817

[Gillespie 1976a] Gillespie, L.K. Burrs produced by drilling. Report BDX-613-1248. Kansas City: Bendix Corp., August 1976

[Gillespie 1976b] Gillespie, L.K. Effects of drilling variables on burr properties. Report BDX-613-1502, 7347654. Kansas City: Bendix Corp., September 1976

[Régnier et al. 2018] Régnier, T., Fromentin, G., Marcon, B., Outeiro, J., D'Acunto, A., Crolet, A., Grunder, T. Fundamental study of exit burr formation mechanisms during orthogonal cutting of AlSi aluminium alloy. Journal of Materials Processing Technology, Jully 2018, Vol.257, pp 112–122, ISSN 09240136

[Rodriguez et al. 2024] Rodriguez, I., Arrazola, P.J., Cuesta, M., Pusavec, F. Hole quality improvement in CFRP/Ti6Al4V stacks using optimised flow rates for LCO2 and MQL sustainable cooling/lubrication. Composite Structures, February 2024, Vol.329, pp 117687, ISSN 02638223